Dalton Transactions

PAPER

Cite this: *Dalton Trans.*, 2015, **44**, 17064

Norharmane rhenium(I) polypyridyl complexes: synthesis, structural and spectroscopic characterization†

Iván Maisuls,[a,b] Ezequiel Wolcan,[a] Oscar E. Piro,[c] Gustavo A. Etcheverría,[c] Gabriela Petroselli,[d] Rosa Erra-Ballsels,[d] Franco M. Cabrerizo*[b] and Gustavo T. Ruiz*[a]

Received 22nd July 2015,
Accepted 30th August 2015

DOI: 10.1039/c5dt02790j

www.rsc.org/dalton

Two novel Re(I) complexes with the general formula *fac*-[Re(CO)$_3$(L)(nHo)]CF$_3$SO$_3$, where L = 2,2′-bipyridine (bpy) or 1,10 phenanthroline (phen) and nHo (9*H*-pyrido[3,4-*b*]indole; norharmane) have been synthesized. The Re(I)–nHo complexes were characterized by structural X-ray diffraction, ^{1}H and ^{13}C NMR, UV-vis absorption and FT-IR spectroscopy, and by a combination of two mass spectrometry techniques, namely ESI-MS and UV-MALDI-MS. All characterizations showed that nHo is coordinated to the metal atom by the pyridine nitrogen of the molecule. X-ray structural analysis revealed that the crystal lattices for both complexes are further stabilized by a strong >N–H···O bond between the pyrrole NH group of the pyridoindole ligand and one oxygen atom of the trifluoromethanesulfonate counter-ion. Ground state geometry optimization by DFT calculations showed that in fluid solution the nHo ligand may rotate freely. The nature of the electronic transitions of Re(CO)$_3$(bpy)(nHo)$^+$ were established by TD-DFT calculations. The set of the most important electronic transitions present in this complex are comprised of $\pi \rightarrow \pi^*$ electronic transitions centered on bpy and nHo moieties, LLCT$_{nHo\rightarrow COs}$, MLLCT$_{Re(CO)_3\rightarrow bpy}$ and LLCT$_{nHo\rightarrow bpy}$ transitions. Additionally, TD-DFT calculations predict the existence of another two intense MLLCT$_{Re(CO)_3\rightarrow nHo}$ electronic transitions. Calculated UV-vis absorption spectra are in good agreement with the corresponding experimental data for the bpy-containing complex.

Introduction

β-Carbolines (βCs) are a group of naturally occurring alkaloids structurally derived from 9*H*-pyrido[3,4-*b*]indole or norharmane (Scheme 1). In nature, βCs are usually found in plants, algae, animals, and are also endogenously synthesized in mammals.[1,2] It has been suggested that these alkaloids would be involved in many biological processes. A large spectrum of psychopharmacological, biological and toxicological activities has been reported for some βCs derivatives, acting as antioxidants, antitumor and antimicrobial agents.[3–5] In some neurodegenerative diseases, such as Alzheimer, quaternary βC derivatives (*i.e.*, those methylated in the pyridinic nitrogen) would play a key role.[6,7]

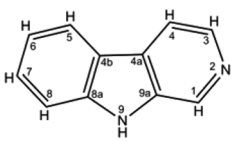

Scheme 1 Schematic chemical structure of 9*H*-pyrido[3,4-*b*]indole.

It is worth mentioning that norharmane, the un-substituted fully aromatic βC, crosses the blood–brain barrier and penetrates into the brain. Inside, norharmane is converted (by certain methyl-transferases) to methyl derivatives exerting significant cyto- and neurotoxic effects.[8,9]

The latter fact seriously reduces the potential medical application of these alkaloids as systemic drugs. Therefore the

[a]*INIFTA, UNLP (CCT La Plata-CONICET), Diag. 113 y 64, C.C. 16, Suc. 4, B1906ZAA La Plata, Argentina. E-mail: gruiz@inifta.unlp.edu.ar*
[b]*IIB-INTECH – UNSAM-CONICET Int. Marino Km 8, 2. CC 164, 7130 Chascomús, Buenos Aires, Argentina. E-mail: fcabrerizo@intech.gov.ar*
[c]*Instituto IFLP (CCT La Plata-CONICET) y Depto. de Física, FCE-UNLP, C. C. 67, 1900 La Plata, Argentina*
[d]*CIHIDECAR-CONICET, Departamento de Química Orgánica, FCEyN, UBA, Pabellón II, 3er P., Ciudad Universitaria, 1428 Buenos Aires, Argentina*
†Electronic supplementary information (ESI) available: Mass spectra (ESI, LDI and MALDI) of the complexes (Fig. S1 and S2), ^{1}H RMN data (Table S1), ionization methods results (Table S2a and b) and TD-DFT calculations results (Tables S3–S5). Tables of fractional coordinates and equivalent isotropic displacement parameters of the non-H atoms (Table S6a and b), full intra-molecular bond distances and angles (Table S7a and b), atomic anisotropic displacement parameters (Table S8a and b) and hydrogen atoms positions (Table S9a and b). CCDC 1038266 and 1038267. For ESI and crystallographic data in CIF or other electronic format see DOI: 10.1039/c5dt02790j

search of novel βC derivatives with non-neurotoxic effects is of keen importance. In this regards, the coordination of these alkaloids to transition metal ions through the pyridinic nitrogen of the βC moiety may represent an excellent option deserving further consideration in future studies. The development of transition metal complexes with coordinated bioactive molecules open up new possibilities in drug discovery. In 1998, Al-Allaf *et al*. synthesized a Pd(II) complex with the natural βC harmine showing great cytotoxic activity against cancer cell lines.[10] Recently, Tan *et al*. synthesized ruthenium(II) transition complexes with norharmane.[11] In these complexes, the βC ligand binds to the metal center through the pyridine nitrogen atom. It has been demonstrated that these βC–Ru(II) complexes have nuclear permeability and can induce autophagy and apoptosis in tumor cells lines. These complexes present great anti-proliferative potential and can associate *in vitro* with DNA. An interesting feature is the enhancement of the βC–Ru complexes fluorescence after the intercalation with DNA.[12] This "*light switch*" effect can be used to monitor the intracellular location of the complex inside a cell. However, as far as we know, there are no examples in the literature of βC–Re(I) complexes. This is surprising since Re(I) tricarbonyl complexes, $XRe(CO)_3L$, continue to attract the attention of researchers due to their applicability in broad research areas such as electron transfer studies,[13] solar energy conversion,[14] catalysis,[15] applications as luminescent molecular probes,[16] *etc*. As these complexes show exceptionally rich excited-state behavior and redox chemistry as well as thermal and photochemical stability,[17,18] they have also been used as biological labeling reagents and non-covalent probes for bio-molecules and ions.[19–21] Furthermore, there are potential biochemical and technical applications based on the formation of adducts between complexes of Re(I) and biological macromolecules such as DNA, proteins or tumor cells.[22–26]

In order to find novel compounds with potential biomedical applications, we undertake the search of new complexes through the combination of $–Re(CO)_3$ moieties with norharmane. We report here the synthesis of two novel Re(I)–nHo complexes, namely $[Re(CO)_3(L)(nHo)]CF_3SO_3$ where L = 2,2′ bypridine, (**1**) or 1,10 phenantroline, (**2**) along with their structural and spectroscopic characterization.

Experimental section

General

HPLC grade methanol and acetonitrile (J. T. Baker, USA), were used without further purification. $Re(CO)_5Cl$, 1,10 phenanthroline (phen), norharmane (nHo) and β-cyclodextrin (cyclomaltoheptaose) were purchased from Sigma-Aldrich Chemical Co., USA. 2,2′-Bipyridine (bpy) and 2-[(2*E*)-3-(4-*tert*-buthylphenyl)-2-methylprop-2-enylidene] malononitrile (DCTB) were purchased from Fluka, Switzerland, toluene from Mallinckrodt Chemicals, tetrahydrofuran (THF) and $HClO_4$ from Merck. Water of very low conductivity (Milli Q grade) was used.

Instrumentation

UV-vis absorption spectra were recorded with a Cary 60 UV-vis spectrophotometer (Agilent Technologies) using methanol as solvent. FTIR spectra were recorded with a Nicolet 8700 Thermo Scientific instrument using KBr pellets. ^{1}H NMR and ^{13}C-NMR spectra were recorded at 300 K with a Bruker AM-500 spectrometer operating at 500 MHz. $[D_6]$DMSO was used as solvent and the chemical shift were internally referenced to TMS *via* $(CH_3)_2SO$ in (δ = 2.50 ppm). *J* values are given in Hz.

Synthesis

1 and **2** were synthesized in a three-step synthesis (see summary in Fig. 1). First, 180.8 mg of $Re(CO)_5Cl$ (0.5 mmol) and 78.1 mg (0.5 mmol) of bpy (for **1**), or 90.1 mg (0.5 mmol) of phen (for **2**) were suspended in 25 mL of toluene and refluxed for 3 h under N_2 atmosphere. After cooling to room temperature, the yellow solid was filtered out and dried under vacuum at 60 °C for 24 h. Later, the solid was dissolved in THF and an equimolar quantity of $AgCF_3SO_3$ was added to the solution and the mixture was refluxed for 4 h under N_2 atmosphere. Then, it was filtered to remove the AgCl formed during the reaction and the solution was rotaevaporated until dryness.

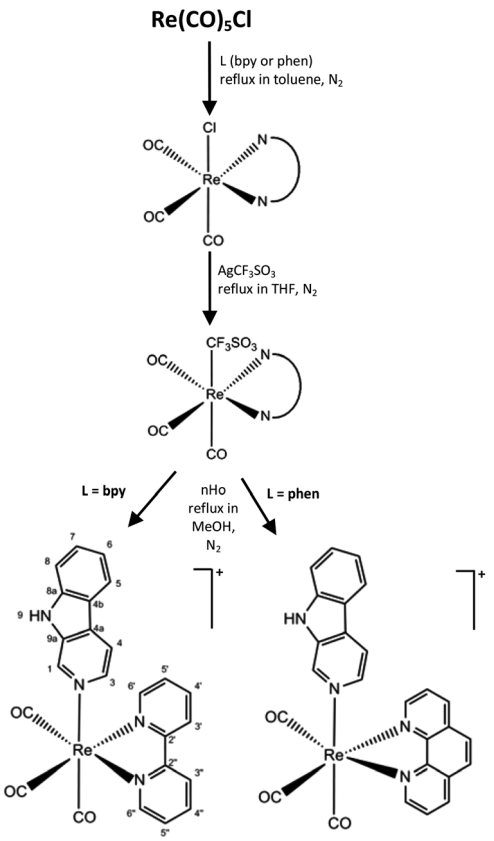

Fig. 1 Synthetic path scheme for *fac*-$[Re(CO)_3(bpy)(nHo)]^+$ and *fac*-$[Re(CO)_3(phen)(nHo)]^+$. The *fac*-$[Re(CO)_3(bpy)(nHo)]^+$ protons have been numbered for the NMR analysis.

The UV-vis absorption spectra of the pure $Re(CO)_3(L)$-CF_3SO_3 obtained herein agreed well with the literature spectra.[27] Finally, these compounds were used as precursors to prepare the desired complexes **1** and **2**. To this purpose, $Re(CO)_3(L)CF_3SO_3$ was suspended in 30 ml of methanol with an equimolar quantity of norharmane and refluxed for 8 h under N_2 atmosphere. After cooling, the solvent was evaporated until dryness and the resulting solid was dried under vacuum at 60 °C for 48 h. The Re(I)–nHo complexes were dissolved in a minimum volume of dichloromethane and then precipitated by slow addition of cold iso-octane. The re-crystallization procedure was repeated until a constant value for the molar absorption coefficient (ε) was obtained. Chemical yields of 75% (**1**, 278.8 mg) and 70% (**2**, 268.7 mg) were obtained in this final step for both complexes. Some Ru(II)–nHo complexes have shown to co-crystallize with solvent molecules.[12,28] In our case, a co-crystallization of solvent molecules was evident from the elemental analysis results.

***fac*-[Re(CO)$_3$(bpy)(nHo)]CF$_3$SO$_3$ (1).** Found: H, 2.65; C, 43.54; N, 7.05%. $C_{25}H_{16}O_6F_3N_4SRe{\cdot}0.45C_8H_{18}$ requires H, 3.06; C, 43.21; N, 7.05%. FT-IR (KBr) ν_{max}/cm^{-1} 1920 and 2031 (CO), 3257 (N9–H). The relevant wavenumbers for nHo are 3419, 1627, 1499, 1467, 1279 and 625 cm^{-1}.

δ_C (500 MHz, d_6-DMSO; TMS) 196.5 (CO), 155.6 (C2′), 154.4 (C2″), 142.3 (C6′), 141.9 (C6″), 141.6 (C5′), 140.4 (C5″), 140.6 (C3), 136.4 (C9a), 140.6 (C8a), 136.6 (C1), 129.6 (C3′), 129.8 (C3″), 129.6 (C4′), 130.7 (C4″), 130.7 (C7), 125.3 (C4b), 123.3 (C4a), 121.0(C6), 123.1 (C5), 112.4 (C8) and 113.2 ppm (C4).

δ_H (500 MHz, d_6-DMSO; TMS) 11.733 (1 H, s, (N)9H), 9.442 (1 H, dd, *J* 5.6, *J* 0.8, C(3′)H), 9.442 (1 H, dd, *J* 5.6, *J* 0.8, C(3″)H), 8.681 (1 H, d, *J* 8, C(6′)H), 8.681 (1 H, d, *J* 8, C(6″)H), 8.542 (1 H, s, C(1)H), 8.406 (1 H, ddd, *J* 7.9, *J* 7.9, *J* 1.4, C(5′)H), 8.406 (1 H, ddd, *J* 7.9, *J* 7.9, *J* 1.4, C(5″)H), 8.232 (1 H, d, *J* 7.8, C(5)H), 8.140 (1 H, d, *J* 5.0, C(3)H), 8.116 (1 H, d, *J* 6, C(4)H), 7.965 (1 H, ddd, *J* 7.7, *J* 5.6, *J* 1.2, C(4′)H), 7.615 (1 H, ddd, *J* 7.7, *J* 5.6, *J* 1.2, C(4″)H), 7.625 (1 H, d, *J* 8, C(8)H), 7.620 (1 H, t, *J* 7.5, C(8)H) and 7.289 (1 H, t, *J* 7.0, C(6)H). The atom numbering and ^{1}H-NMR data for both complex **1** and free nHo are shown in Table S1.†

***fac*-[Re(CO)$_3$(phen)(nHo)]CF$_3$SO$_3$] (2).** Found: H, 1.71; C, 40.50; N, 5.82%. $C_{27}H_{16}O_6F_3N_4SRe{\cdot}0.9\ CH_2Cl_2$ requires H, 2.13; C, 39.70; N, 6.60%. FT-IR (KBr) ν_{max}/cm^{-1} 1915 and 2013 (CO) and 3260 (N9–H).

Mass spectrometry analysis

HRESI-MS analysis. High resolution electrospray ionization (HRESI) mass spectrometry (MS) analysis was performed in positive ion mode using the mass spectrometer BRUKER microTOF-Q II equipped with CID. Acquisition parameters: capillary temperature, 180 °C; nebulizer pressure, 0.4 Bar; capillary voltage, 4500 V; dry heater temperature, 200 °C; end plate offset voltage, −450 V; set dry gas at 4.0 l min^{-1}; collision cell RF, 150.0 Vpp. Stock solutions of the Re(I)–nHo complexes were prepared in methanol at a concentration 10^{-4} M. When formic acid was added to the methanolic complex solutions the molecular ions were not detected. Diluted solutions were prepared from the stock solutions.

MALDI-TOF/TOF MS analysis. The Re(I)–nHo complexes were analyzed by ultraviolet matrix assisted laser desorption–ionization mass spectrometry (UV–MALDI MS) performed on the Bruker Daltonics Ultraflex II TOF/TOF mass spectrometer (Leipzig, Germany). Mass spectra were acquired in linear positive and negative ion modes and with the LIFT device in the MS/MS mode. Stock solutions of complexes (10^{-4} M) were prepared in methanol. These solutions were then diluted 10 to 100-fold to a final concentrations 10^{-5} to 10^{-6} M. External mass calibration was made using β-cyclodextrin (MW 1134) with norharmane as matrix in positive and negative ion mode. The matrix signal was used as an additional standard for calibration in both ionization modes. Sample solutions were spotted on a MTP 384 polished stainless steel target plate from Bruker Daltonics (Leipzig, Germany). Matrix solutions were prepared by dissolving nHo (1 mg ml^{-1}) in acetonitrile/water (1 : 1, v/v) solution and DCTB[29,30] (10 mg ml^{-1}) in dichloromethane. For UV-MALDI MS experiments sandwich method was used according to Nonami *et al.*,[31] *i.e.*, loading successively 0.5 μl of matrix solution, analyte solution and matrix solution after drying each layer at normal atmosphere and room temperature. Desorption/ionization was obtained by using the frequency-tripled Nd:YAG laser (355 nm). Spectra were obtained and analyzed with the programs FlexControl and FlexAnalysis, respectively.

X-Ray diffraction data

Single crystals suitable for X-ray diffraction analysis for both complexes were obtained by a slow evaporation from methanol/hexane solutions. The measurements of *fac*-$[Re(CO)_3(phen)(nHo)]CF_3SO_3$ crystal were performed on an Oxford Xcalibur, Eos, Gemini CCD diffractometer with graphite-monochromated MoKα (λ = 0.71073 Å) radiation. X-ray diffraction intensities were collected (ω scans with ϑ and κ-offsets), integrated and scaled with CrysAlisPro[32] suite of programs. The unit cell parameters were obtained by least-squares refinement (based on the angular settings for all collected reflections with intensities larger than seven times the standard deviation of measurement errors) using CrysAlisPro. Data were corrected empirically for absorption employing the multi-scan method implemented in CrysAlisPro. The *fac*-$[Re(CO)_3(bpy)(nHo)]$-CF_3SO_3 crystal was measured with an Enraf-Nonius Kappa-CCD diffractometer employing graphite-monochromated MoKα radiation. Diffraction data were collected (φ and ω scans with κ-offsets) with COLLECT.[33] Integration and scaling of the reflections was performed with HKL DENZO-SCALEPACK[34] suite of programs. The unit cell parameters were obtained by least-squares refinement based on the angular settings for all collected reflections using HKL SCALEPACK.[34] Data were corrected numerically for absorption with PLATON[35] and also for extinction effects. The structures were solved by direct methods with SHELXS of the SHELX package[36] and the molecular model developed by alternated cycles of Fourier methods and full-matrix least-squares refinement with SHELXL of the same suit of

programs. The H-atoms of the organic ligand were positioned stereo chemically and refined with the riding model. The *fac*-[Re(CO)$_3$(phen)(nHo)]CF$_3$SO$_3$ crystal showed disordered solvent which could not be modeled satisfactory in terms of the expected solvent molecules. Therefore, it was resorted to SQUEEZE[37] procedure to eliminate from the diffraction data the contribution due to this disordered electron density followed by the refinement of the ordered part. In *fac*-[Re(CO)$_3$(bpy)(nHo)]-CF$_3$SO$_3$ crystal the CF$_3$SO$_3^-$ counter-ion showed appreciable positional disorder and all but the carbon atom were treated anisotropically. Crystal data and structure refinement results for *fac*-[Re(CO)$_3$(L)(nHo)]CF$_3$SO$_3$ (L = bpy, phen) are in Table 1. Full crystallographic data have been deposited at the Cambridge Crystallographic Data Centre (CCDC). Any request to the CCDC for this material should quote the full literature citation and the reference number CCDC 1038266 (phen) and CCDC 1038267 (bpy).

Computational details

DFT and TD-DFT calculations of ground and excited state properties of a series of Re(I) tricarbonyl complexes have been recently employed to interpret the experimental UV-vis absorption bands due to a set of MLCT, LLCT and IL transitions.[38] The ligand nHo coordinated to Re by the pyridine N (N-2) may adopt different orientations, hence generating conformational isomers. These conformers only differ in the direction of the pyrrolic NH group (N-9). DFT calculations were performed in order to elucidate if there is any preferential orientation (lower energy state) for these conformers. DFT calculations on the electronic structure of the complexes were carried out with Gaussian 09 software.[39–42] Ground state geometry optimization was performed on two conformers of [Re(CO)$_3$(bpy)(nHo)]$^+$ (named hereafter Re-1 and Re-2, see Fig. 2) with the B3LYP hybrid functional using the LanL2DZ basis set.[43–46]

Vibration frequencies were computed at the same level of theory to confirm that these structures were minima on the energy surfaces. The cartesian coordinates corresponding to the X-ray structure were used as starting positions in the optimization process of the Re-1 structure. In this conformer the coordinated nHo molecule lies onto a plane bisecting both N–Re–C angles. On the other hand, in the Re-2 conformer, the coordinated nHo molecule is rotated 90° respect to its position

Table 1 Crystal data and structure refinement results for of *fac*-[Re(CO)$_3$(L)(nHo)]CF$_3$SO$_3$ (L = phen, bpy) complexes

Compound	**L** = phen	**L** = bpy
Empirical formula	C_{27} H_{16} F_3 N_4 O_6 Re S	C_{25} H_{16} F_3 N_4 O_6 Re S
Formula weight	767.70	743.68
Temperature (K)	295(2)	295(2)
Wavelength (Å)	0.71073	0.71073
Crystal system	Monoclinic	Trigonal
Space group	$P2_1/n$	$P3_1$
Unit cell dimensions		
a (Å)	11.7831(2)	15.1660(9)
b (Å)	13.8328(3)	15.1660(9)
c (Å)	17.5603(3)	9.9800(7)
α (°)	90.00	90.00
β (°)	94.139(2)	90.00
γ (°)	90.00	120.00
Volume (Å^3)	2854.75(9)	1987.9(2)
Z, density (calculated, mg m^{-3})	4, 1.786	3, 1.864
Absorption coefficient (mm^{-1})	4.397	4.732
F(000)	1508	1080
Crystal shape/color	Fragment/yellow	Fragment/yellow
Crystal size (mm^3)	0.331 × 0.194 × 0.183	0.211 × 0.066 × 0.059
θ-range (°) for data collection	2.95 to 27.00	2.69 to 25.99
Index ranges	$-15 \le h \le 14$, $-16 \le k \le 17$, $-20 \le l \le 22$	$-18 \le h \le 18$, $-18 \le k \le 18$, $-12 \le l \le 12$
Reflections collected	16 412	10 339
Independent reflections	6159 [R(int) = 0.0317]	5145 [R(int) = 0.0624]
Observed reflections [$I > 2\sigma(I)$]	4988	4106
Completeness (%)	99.0 (to θ = 27.00°)	99.8 (to ϑ = 25.995°)
Absorption correction	Semi-empirical from equivalents	Numerical
Max. and min. transmission		0.7676 and 0.4351
Refinement method	Full-matrix least-squares on F^2	Full-matrix least-squares on F^2
Data/restraints/parameters	6163/0/379	5145/1/357
Goodness-of-fit on F^2	1.052	0.984
Final R indices[a] [$I > 2\sigma(I)$]	R_1 = 0.0305, wR_2 = 0.0773	R_1 = 0.0537, wR_2 = 0.1390
R indices (all data)	R_1 = 0.0441, wR_2 = 0.0833	R_1 = 0.0648, wR_2 = 0.1457
Extinction coefficient		0.029(2)
Absolute structure parameter		−0.02(2)
Largest diff. peak and hole (e Å^{-3})	1.686 and −0.574	1.444 and −1.038

[a] $R_1 = \sum||F_o| - |F_c||/\sum|F_o|$, $wR_2 = [\sum w(|F_o|^2 - |F_c|^2)^2/\sum w(|F_o|^2)^2]^{1/2}$.

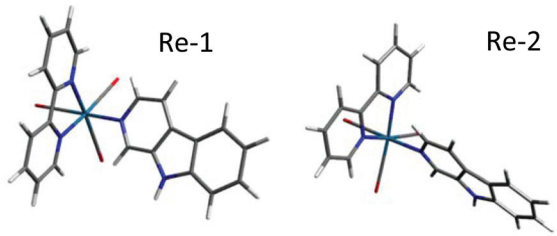

Fig. 2 Re-1 and Re-2 conformers of $[Re(CO)_3(bpy)(nHo)]^+$.

in the Re-1 conformer, bisecting now the N–Re–N and C–Re–C angles. The energies of the vertical electronic transitions were computed at the optimized geometry of the ground-state by TD-DFT.[47–49] The number of calculated singlet-to-singlet electronic transitions was 110. Both optimized geometries and TD-DFT calculations were carried out including solvent (MeOH) effects through the Polarizable Continuum Model (PCM).[50–52] Output files from Gaussian 09 were analyzed with the AOMix program to obtain the percentage compositions of different molecular fragments to molecular orbitals (MOs). GaussSum 2.2.5 program was used to simulate absorption spectra with Gaussian distributions with a full-width at half-maximum (fwhm) set to 3000 cm^{-1}.

Results and discussion

Spectroscopic characterization

The $[Re(CO)_3(L)(nHo)]CF_3SO_3$ (L = bpy or phen) complexes were obtained in good yields and fully characterized by elemental analysis, FTIR and NMR spectroscopy (^1H and ^{13}C), MALDI and HRESI mass spectrometry.

Structural X-ray diffraction methods were used on single crystals obtained for both complexes. The FTIR absorption spectra of the complexes are consistent with both the facial configuration of the carbonyl ligands and with their C_s symmetry, as revealed by the presence of two intense absorption bands in the 2100–1800 cm^{-1} region. According to previous reports on similar compounds, the sharp band at higher frequency (*ca.* 2031 and 2030 cm^{-1} to L = bpy and phen, respectively) is attributed to the A′1 mode (the in-phase totally symmetric stretch of the three CO ligands).[53] The spectra show other broad band (*ca.* 1920 and 1915 cm^{-1} to L = bpy and phen, respectively) which can be assigned to the A′2 (totally symmetric out-of-phase stretching) and A″ modes (asymmetric stretching of the equatorial carbonyls ligands). In fact, A′2 and A″ bands, have already been observed as bands superimposed into a single broad band in *fac*-$[Re(CO)_3(NN)(R\text{-pyridyl})]^+$ complexes, where the environment of Re is more symmetric (Re bound to three CO and three pirydinic nitrogen) than other Re (I) tricarbonyl complexes (*e.g. fac*-$[Re(CO)_3(NN)(L)]$, L = halide, $CF_3SO_3^-$, *etc.*).[54–56] The patterns observed in the obtained complexes are in agreement with the high symmetry expected around the metal center due to the coordination of nHo ligand by pyridine N (N-2) as shown by the X-ray results (see below).

Compared to the free norharmane ligand, the FTIR spectra of the complexes showed slight shift to upper frequencies in the region 1200–1700 cm^{-1} ($\Delta\nu$ < 10 cm^{-1}). Most remarkable differences were observed on N–H peak of nHo ligand in the complexes (N9–H). While N–H peak of free nHo is observed at 3419 cm^{-1} the complexes showed significant shifts to lower frequencies (3257 and 3260 cm^{-1} to bpy and phen, respectively) These shifts are typical features that indicate that norharmane is coordinated to the metal core in a similar way to that reported recently for Ag(I)–nHo complexes.[57]

HRESI-MS and UV-MALDI-MS

Mass spectrometry was used to study the molecular structure of rhenium complexes. Fig. S1† shows the HRESI mass spectrum in positive ion mode of the complex $[Re(CO)_3(bpy)(nHo)]$-CF_3SO_3. The intact cationic moiety belonging to the molecular ion, $[Re(CO)_3(bpy)(nHo)]^+$, as $[M]^+$ at m/z = 595.08, the fragment formed when a CO ligand is lost $[M - (CO)]^+$ at m/z = 566.88 and the one formed when nHo ligand is lost $[M - (nHo)]^+$ at m/z = 427.00 were observed. Additionally, a signal at m/z = 169.08 was detected, corresponding to nHo ligand. As mentioned by Wyatt in a recent review[29] ESI-MS has been more used for the analysis of organometallic complexes than UV-MALDI-MS, however there are instances when both techniques may be used in a complementary fashion. Furthermore, it is necessary to expand previous studies of organometallic compounds using UV-MALDI-MS to obtain information of new compounds that could act as efficient matrices. Since $[Re(CO)_3(bpy)(nHo)]CF_3SO_3$ complex shows strong absorption in the UV-vis region (see below), particularly at 355 nm, laser desorption ionization mass spectrometry (LDI-MS), without needing the presence of a secondary molecule as photosensitizer or matrix in the sample, was used. It is worth noticing that previously nHo has been used as MALDI matrix for the detection of organometallic compounds.[30] As shown in Fig. S1,† intact cation moiety of the molecular ion of this complex could be detected in positive ion mode but the signal obtained was very weak. Additionally, two more structure diagnosis signals were obtained when comparing with the ESI spectrum described before, $[M - 3(CO)]^+$ at m/z = 511.16 and $[M - (CO) - (nHo)]^+$ m/z = 399.06. MALDI mass spectra of $[Re(CO)_3(bpy)$-$(nHo)]CF_3SO_3$ complex were recorded using DCTB and nHo as matrices. Both matrices have been previously used for analysis of rhenium complexes.[30,58] Fig. S1† shows the spectrum recorded using DCTB as matrix. Similar results were obtained when nHo was used (result not shown). Some fragments produced by the loss of one or more ligands were observed using both techniques but as UV-MALDI-MS is a softer ionization technique than LDI-MS it was possible to detect the intact molecular ion of the complex under study with better signal-to-noise ratio. All ionization methods used allowed to detect the intact molecular ion. However, the total intensity for signal at m/z = 595.08 was higher when ESI was used instead of MALDI.

Fig. S2† shows ESI mass spectrum in positive ion mode of the complex $[Re(CO)_3(phen)(nHo)]CF_3SO_3$. The intact cation moiety of the molecular ion was detected as $[M]^+$ at m/z = 619.07 together with the one formed when nHo ligand is lost $[M - (nHo)]^+$ at m/z = 451.00. LDI and MALDI mass spectra showed similar signals. The intact cation moiety of the molecular ion was detected with better signal-to-noise ratio in MALDI compared with LDI experiment. Additionally, the fragments formed when one or more CO and/or nHo ligands were lost, $[M - (CO)]^+$ at m/z = 591.17, $[M - 3(CO)]^+$ at m/z = 535.17, $[M - (nHo)]^+$ at m/z = 451.08 and $[M - (CO)(nHo)]^+$ at m/z = 423, were respectively observed. Table S2a and S2b† show the most representative ions related to the Re(I)–nHo complexes observed with the different ionization methods used in this work. Finally, it is interesting to mention that when formic acid was added to the methanolic complex solutions used in the ESI-MS experiments, the molecular ions were not detected in agreement with the fact that the protonated nHo pyridine N yielded in the presence of formic acid is the same nHo pyridine N involved in the Re–nHo linkage, which is destroyed in acidic medium.

Structural characterization

Fig. 3 and 4 are ORTEP[59] plots of solid state *fac*-$[Re(CO)_3(L)(nHo)]CF_3SO_3$ (L = phen, bpy) showing that both complexes are structurally closely related to each other by interchange of the phenanthroline and bipyridine bidentate ligands. Intra-molecular bond distances and angles around the metal are compared in Table 2. We shall discuss the structure of the better refined phenanthroline-containing complex.

Rhenium(I) ion is in a slightly distorted octahedral environment, *cis*-coordinated to three carbonyl (CO) groups [Re–C distances in the range from 1.919(6) to 1.930(4) Å, *cis* C–Re–C angles in the 86.3(2)–89.6(2)° interval; C–O from 1.132(5) to 1.151(6) Å and Re–C–O angles in the 176.2(5)–178.0(4)° range].

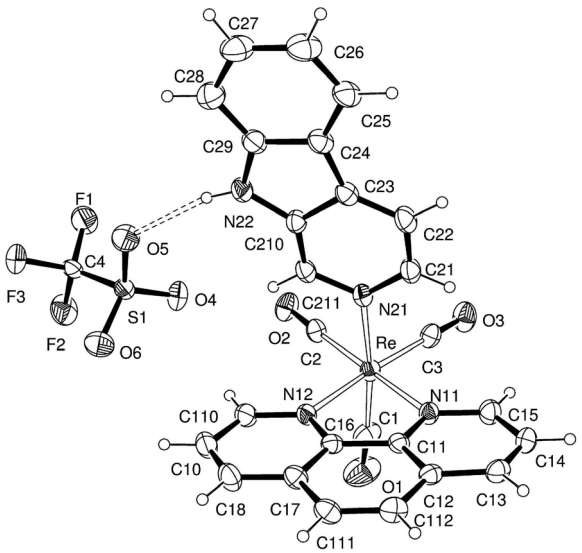

Fig. 3 View of *fac*-$[Re(CO)_3(phen)(nHo)]CF_3SO_3$ showing the labeling of the non-H atoms and their displacement ellipsoids at the 30% probability level. Metal–ligand bonds are indicated by open lines and the intermolecular H-bond by dashed lines.

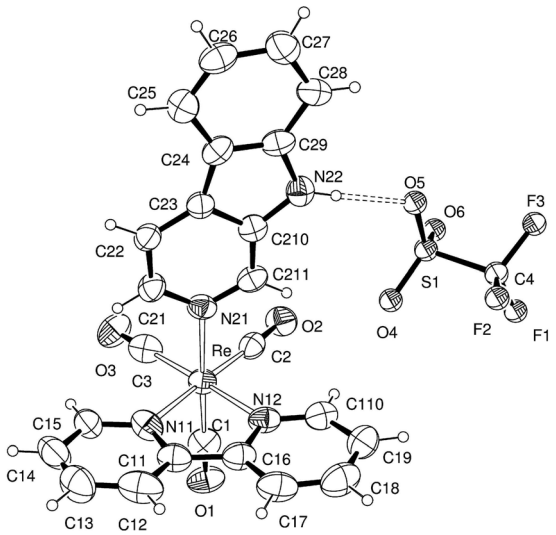

Fig. 4 View of *fac*-$[Re(CO)_3(bpy)(nHo)]CF_3SO_3$ in the solid. The isotropic atomic displacement parameter for the disordered $CF_3SO_3^-$ counter-ion has been arbitrarily set to 0.05 Å^2.

Table 2 Bond lengths [Å] and angles [°] around rhenium ion for *fac*-$[Re(CO)_3(L)(nHo)]CF_3SO_3$ (L = phen, bpy) complexes

L: phen		L: bpy	
Re–C(1)	1.919(6)	Re–C(1)	1.93(3)
Re–C(2)	1.930(4)	Re–C(2)	1.84(2)
Re–C(3)	1.923(5)	Re–C(3)	1.93(3)
Re–N(11)	2.187(3)	Re–N(11)	2.20(2)
Re–N(12)	2.176(4)	Re–N(12)	2.19(2)
Re–N(21)	2.207(3)	Re–N(21)	2.23(2)
C(1)–Re–C(3)	89.6(2)	C(1)–Re–C(3)	88.2(9)
C(1)–Re–C(2)	87.9(2)	C(2)–Re–C(1)	88.2(8)
C(3)–Re–C(2)	86.3(2)	C(2)–Re–C(3)	84.7(9)
C(1)–Re–N(12)	91.5(2)	C(1)–Re–N(12)	93.6(7)
C(3)–Re–N(12)	173.5(1)	C(3)–Re–N(12)	175.0(8)
C(2)–Re–N(12)	100.2(2)	C(2)–Re–N(12)	99.9(7)
C(1)–Re–N(11)	97.1(2)	C(1)–Re–N(11)	94.3(7)
C(3)–Re–N(11)	97.8(2)	C(3)–Re–N(11)	100.2(8)
C(2)–Re–N(11)	173.6(2)	C(2)–Re–N(11)	174.5(7)
N(12)–Re–N(11)	75.7(1)	N(12)–Re–N(11)	75.1(6)
C(1)–Re–N(21)	173.1(2)	C(1)–Re–N(21)	178.1(7)
C(3)–Re–N(21)	96.8(2)	C(3)–Re–N(21)	93.5(7)
C(2)–Re–N(21)	90.0(2)	C(2)–Re–N(21)	92.6(7)
N(12)–Re–N(21)	82.4(1)	N(12)–Re–N(21)	84.6(6)
N(11)–Re–N(21)	84.6(1)	N(11)–Re–N(21)	84.7(6)

Two other *cis*-positions are occupied by the N-atoms of a phenanthroline molecule acting as bidentate ligand through its N-atoms [Re–N bond distances of 2.176(4) and 2.187(3) Å] and defining an equatorial coordination plane nearly containing the Re(I) ion and two of the above CO ligand groups. The six-fold coordination is completed by a planar nHo molecule [rms deviation of atoms from the best least-squares plane of

0.0128 Å with the metal 0.052(4) Å apart] acting as monodentate ligand through its pyridine N-atom [d(Re–N) = 2.207(3) Å]. As shown in Fig. 3 and 4, both lattices are further stabilized by a strong >N–H···O bond between the pyrrole NH group on the pyrido indole ligand and one oxygen atom of the trifluoromethanesulfonate counter-ion [N···O distances of 2.94 Å (phen) and 2.84 Å (bpy), and N–H···O angles of 166° (phen) and 176° (bpy)]. Crystal structure of *fac*-[$Re(CO)_3$(bpy)(nHo)]-CF_3SO_3 suggests the stabilization of Re-1 conformer in the solid phase as a consequence of this H-bridge.

UV-vis absorption spectroscopy

The UV-vis absorption spectra of [$Re(CO)_3$(L)(nHo)]CF_3SO_3 complexes in MeOH solutions (Fig. 5) present similar features and thus they will be discussed together. They consist of three different groups of absorption bands. In the first group appear the most intense bands ($\varepsilon \sim 4$–4.5×10^4 M^{-1} cm^{-1}). For [$Re(CO)_3$(bpy)(nHo)]$^+$ those bands are centered at λ_{max} = 241 and 249 nm and a shoulder appears at 261 nm. For [$Re(CO)_3$(phen)(nHo)]$^+$ the position of the most intense bands are somewhat red-shifted with λ_{max} = 252 nm and a shoulder at 273 nm. The second group is less intense than those of the first group ($\varepsilon \sim 2.5$–3×10^4 M^{-1} cm^{-1}): peaks at λ_{max} = 306 nm with a shoulder at 319 nm for [$Re(CO)_3$(bpy)(nHo)]$^+$ and λ_{max} = 301 nm for [$Re(CO)_3$(phen)(nHo)]$^+$ respectively. The weakest bands ($\varepsilon \sim 8$–9×10^3 M^{-1} cm^{-1}) are observed between 320 and 450 nm, *i.e.*, for [$Re(CO)_3$(bpy)(nHo)]$^+$ one band peaking at λ_{max} = 355 nm with a shoulder at 368 nm are observed. Those bands are nearly identical for [$Re(CO)_3$(phen)(nHo)]$^+$ complex, both in position and intensity. For both complexes, a long tail extending from 400 to 450 nm indicates the existence of at least another absorption band with λ_{max} in the 370–400 nm interval. For comparative purposes, Fig. 5 also shows the absorption spectrum of nHo in methanolic solution with $HClO_4$ (nHo in the protonated form, $nHoH^+$).[60] Additionally, electronic absorption data were summarized in Table 3 in order to facilitate the comparison.

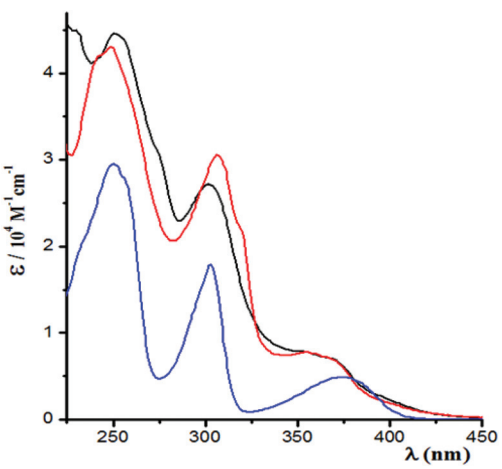

Fig. 5 UV-vis absorption spectra of [$Re(CO)_3$(bpy)(nHo)]CF_3SO_3 (red), [$Re(CO)_3$(phen)(nHo)]CF_3SO_3 (black) in MeOH, and $nHoH^+$ (blue, nHo in MeOH + $HClO_4$).

Table 3 Electronic absorption data, λ/nm ($\varepsilon/10^3$ M^{-1} cm^{-1}), of both complexes in MeOH, and $nHoH^+$ (nHo in MeOH + $HClO_4$). ε values were determined within 10% error

[$Re(CO)_3$(bpy)(nHo)]CF_3SO_3	[$Re(CO)_3$(phen)(nHo)]CF_3SO_3	$nHoH^+$
368 (6.9)	368 (5.9)	371 (4.3)
355 (7.9)	355 (6.7)	301 (15.0)
319 (22.5)	301 (23.7)	248 (27.3)
306 (31.5)	275 (26.7)	215 (15.3)
249 (44.5)	252 (39.1)	
241 (43.3)	230 (40.0)	

The UV-vis absorption spectra of both [$Re(CO)_3$(L)(nHo)]-CF_3SO_3 complexes showed significant spectroscopic differences respect to the sum of the $nHoH^+$ and [$Re(CO)_3$(L)]-CF_3SO_3 individual absorption spectra. Those new spectral features were used to identify the coordination of nHo ligand during the reaction. In particular, the new band that arises a $\lambda \sim 305$ nm in the absorption spectra of both complexes is not present in the absorption spectra of the precursors.[27] On the other hand, this band shows features similar to the ones observed in the spectrum of protonated norharmane, suggesting mono-dentate coordination to the metal core by the pyridine N-atom. In addition, the absorptions observed between 350–450 nm suggests also new charge transfer transitions bands by coordination of nHo. In order to get a deeper understanding of the absorption spectrum of [$Re(CO)_3$(L)(nHo)]CF_3SO_3 complexes, in terms of a set of MLCT, LLCT and IL electronic transitions, DFT and TD-DFT calculations were performed for the [$Re(CO)_3$(bpy)(nHo)]$^+$ complex and the results are presented in the next sections.

Quantum chemistry of [$Re(CO)_3$(bpy)(nHo)]$^+$

DFT calculations. Ground state geometry optimization results on two Re-1 and Re-2 conformers of [$Re(CO)_3$(bpy)-(nHo)]$^+$, Fig. 2, provide additional structural information. The accuracy of these calculations were monitored by comparing them with the corresponding X-ray crystallographic data obtained for Re(I) tricarbonyl complex. The theoretical values for selected bond distances and angles for Re-1 and Re-2 are shown in Table 4. They are in good agreement with those obtained by X-ray diffraction, with bond lengths differing in less than 0.1–0.2 Å and bond angles by 3° or less. From the comparison of the sum of electronic energy plus zero point energy for both conformers it is concluded that Re-1 is more stable than Re-2 in about 0.8 Kcal mol^{-1}. Though intermediate conformations of [$Re(CO)_3$(bpy)(nHo)]$^+$ with different angles of the nHo ligand between those in Re-1 and Re-2 conformers were not examined, it is highly probable that in fluid solution the ligand nHo molecule may rotate freely (remember also that $kT \sim 0.6$ Kcal mol^{-1} at 298 K).

To interpret the nature of the experimental UV-vis absorption bands, TD-DFT calculations were performed on the opti-

Table 4 Bond lengths [Å] and angles [°] around the Re ion in $[Re(CO)_3(bpy)(nHo)]^+$ [a]

Bond length	X-Ray [Å]	Re-1 [Å]	Re-2 [Å]
C2–O2	1.263	1.189	1.189
C3–O3	1.163	1.183	1.189
C1–O1	1.153	1.188	1.188
Re–C1	1.933	1.925	1.923
Re–C2	1.842	1.924	1.924
Re–C3	1.933	1.925	1.925
Re–N21	2.232	2.229	2.237
Re–N11	2.202	2.179	2.182
Re–N12	2.192	2.179	2.183
Angles	[°]	[°]	[°]
C1–Re–N21	178.17	176.56	178.28
C2–Re–N11	174.57	172.87	172.64
N12–Re–N21	84.66	84.90	91.06
N11–Re–N12	75.07	75.56	75.31
N11–Re–N21	84.76	85.00	87.61
C1–Re–N12	93.67	92.17	91.02
C2–Re–N12	99.97	97.81	97.21
C2–Re–N21	92.67	91.97	91.31
C3–Re–N11	100.28	97.51	97.41
C3–Re–N21	93.57	92.11	91.06

[a] Note that the crystallographic numbering (Fig. 3 and 4) differs from the numbering according to the heterocyclic nomenclature (Fig. 1).

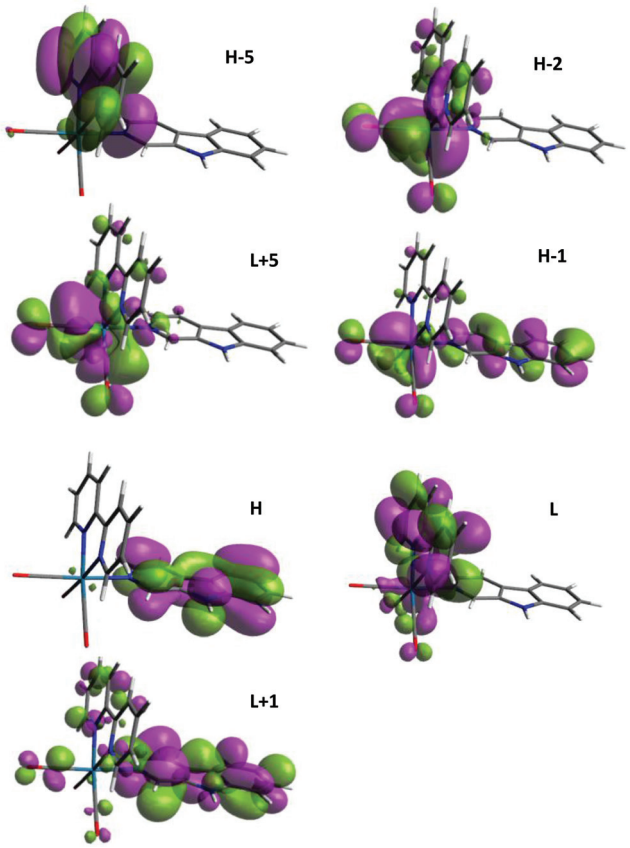

Fig. 6 Spatial plots of most representative MOs in **Re-1** conformer.

mized structures of Re-1 and Re-2 conformers at the B3LYP/LanL2DZ/PCM level of theory. The TD-DFT results are summarized in Table S3† where they are compared with the corresponding experimental data. The MOs which are mainly responsible for the electronic transitions observed in the absorption spectrum of the Re(I) complex within the 220–500 nm wavelength range are: HOMO, LUMO, and the groups of MOs H−8 through H−1 and L+1 through L+7. The percentage compositions of those MOs were obtained from Mulliken population analysis with the aid of AOMIX program from contributions of four fragments, namely: (i) Re atom, (ii) the three carbonyls, (iii) bpy molecule and (iv) nHo molecule. Fig. 6 and 7 show the spatial plots of a selection of those MOs most representative in Re-1 and Re-2 conformers, respectively. Tables S4 and S5† show the calculated % compositions of all fragments at each MO for Re-1 and Re-2 along with % composition vs. Energy plots.

We give below a brief description of relevant MOs of Re-1 in terms of the fragments percentage compositions. H and H−6 are bonding MOs almost exclusively composed (>99% character) of nHo molecule π-orbitals.

In H−1 the charge density distribution is mainly concentrated on nHo (54%), Re (29%) and COs (13%), with a very small contribution of bpy (3%) to that MO. H−5 and H−7 are bonding MOs of π character exclusively centered on bpy (>95% character). H−3 and H−4 are bonding MOs mainly centered on the Re atom (54% and 45% character, respectively) with smaller contributions of COs and nHo (between 20 and 30%) and even smaller (~4%) contributions of bpy orbitals. H−2 consists mainly in Re (63%) and COs (28%) orbitals. LUMO, L+2 and L+3 are anti-bonding orbitals exclusively centered on bpy fragment. L+1 is an anti-bonding MO nearly exclusively centered on nHo fragment (87% composition) with a smaller participation of bpy (8%) and COs (4%) fragments. L+4 and L+5 are antibonding MOs mainly centered on the COs fragments (75%) with around 20% contribution of Re atom. L+6 is an antibonding MO mainly centered on nHo fragment (67%) with 28% of contribution from COs. L+7, on the other hand, is an antibonding MO mainly centered on COs fragments (70%) with 27% of contribution from nHo. MOs orbitals of Re-2 are very similar in nature to those of Re-1. The only significant difference arises in H−3 of Re-2: a bonding MO mainly centered on the nHo fragment (58%) with around 26% contribution of Re atom, 11% of COs and 5% of bpy.

Since the simulated absorption spectrum derived from TD-DFT calculations on Re-2 gave much better agreement (see below) than that of Re-1 when compared with experimental data for $[Re(CO)_3(bpy)(nHo)]^+$ in MeOH, only TD-DFT calculated electronic transitions of Re-2 will be discussed in detail. However, the most significant differences between TD-DFT calculated electronic transitions of Re-2 and Re-1 will be highlighted later below. In general, for Re-2 it is observed that the main spectral features are predicted by TD-DFT calculations with good accuracy, both in position and relative intensities.

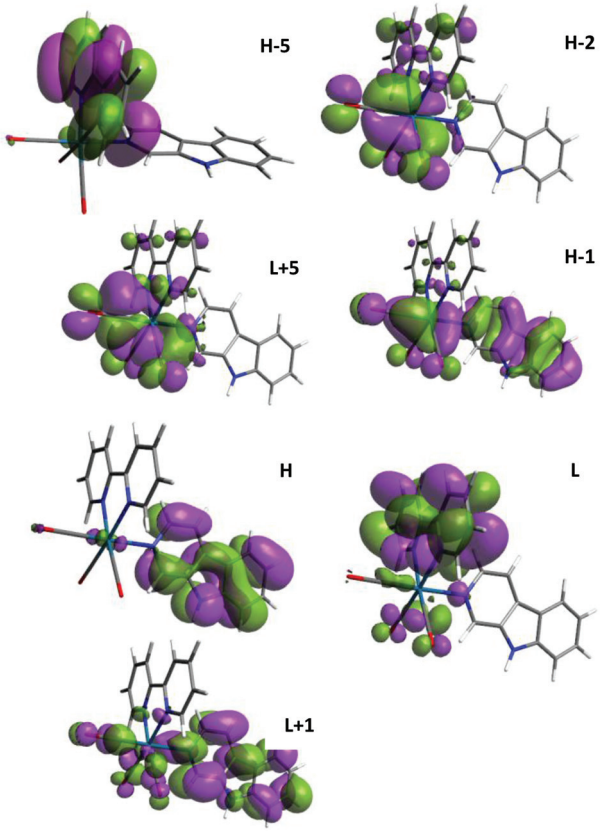

Fig. 7 Spatial plots of most representative MOs in **Re-2** conformer.

In the 220–300 nm wavelength region, the two observed high intensity bands centered at λ_{max} = 241 and 249 nm (the latter with a shoulder at 261 nm) are predicted by TD-DFT as a set of five electronic transitions (see Table S3b,† yellow highlighted). H−5 → L+2 and H−6 → L+1 are π → π* electronic transitions centered in bpy and nHo fragments, respectively. The most intense electronic transitions are H → L+6 and H → L+7, which are $LLCT_{nHo\rightarrow COs}$ electronic transitions. H−3 → L+4 is an admixture of $LLCT_{nHo\rightarrow COs}$ and $MLCT_{Re\rightarrow COs}$ electronic transitions. The spectral features observed in the absorption spectrum of $[Re(CO)_3(bpy)(nHo)]^+$ between 300 and 320 nm (a medium intensity band centered at λ_{max} = 306 nm with a shoulder at 319 nm) are predicted by TD-DFT as a series of four electronic transitions (see Table S3b,† green highlighted). The most intense, *i.e.* H−1 → L+1, is a $MLLCT_{Re(CO)_3\rightarrow nHo}$ electronic transition. H−4 → L+1 is also a $MLLCT_{Re(CO)_3\rightarrow nHo}$ electronic transition. H−5 → L is a π → π* electronic transition centered on bpy. H−1 → L+3 is an admixture of a $MLLCT_{Re(CO)_3\rightarrow bpy}$ and a $LLCT_{nHo\rightarrow bpy}$ electronic transitions. Finally, in the lowest energy region, the observed absorption band at λ_{max} = 355 nm with a shoulder at 368 nm are predicted by TD-DFT as two electronic transitions (see Table S3b,† grey highlighted). H → L+1 is mainly a π → π* electronic transition of nHo. H−4 → L, however, is a $MLLCT_{Re(CO)_3\rightarrow bpy}$ electronic transition. The calculated electronic spectra of $[Re(CO)_3(bpy)(nHo)]^+$ is simulated from the theoretical results to ease the comparison with experimental data. The simulations are shown in Fig. 8 in comparison with the experimental absorptions. It is observed that the simulated spectrum for Re-2 compares very well with the experimental one.

The comparison of the experiments with the simulated spectrum for Re-1 is not so good since Re-1 spectrum fails to reproduce the experimental absorption spectrum in the 350–400 nm wavelength region and reproduces poorly the bands at λ_{max} = 306 nm and the shoulder at 319 nm. However, Re-1 spectrum reproduces quite well the high energy bands and it also gives a good account of the observed long tail spreading between 400 and 450 nm. Since, as noted above, both conformers differ in the sum of electronic plus zero point energies in a small energy amount, in fluid solutions there may be a rapid interchange between many possible conformations and thus the observed absorption spectrum could be a time-averaging of all of them. The main difference between Re-1 and Re-2 TD-DFT calculations appears in the 300–450 nm wavelength region. H−1 → L is the only calculated electronic transition with significant intensity in the lowest energy region, which corresponds to an admixture of $MLLCT_{Re(CO)_3\rightarrow bpy}$ and a $LLCT_{nHo\rightarrow bpy}$ electronic transitions (see Table S3a,† yellow highlighted). In the 300–325 nm spectral region, both

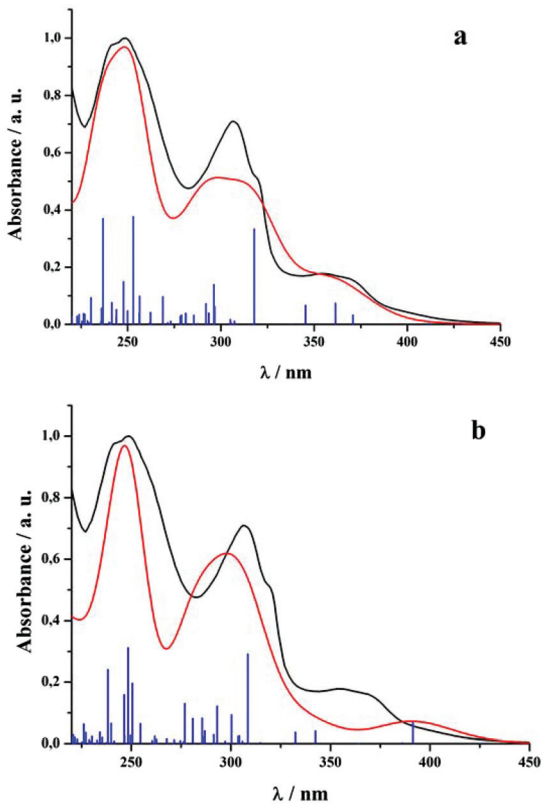

Fig. 8 Comparison of the UV–vis absorption spectrum (black curves) with TD-DFT calculated electronic transitions (blue lines) and simulated spectra (red curves) for (a) **Re-2**/PCM/MeOH and (b) **Re-1**/PCM/MeOH conformers.

conformers Re-1 and Re-2 display a high intensity calculated electronic transition which defines the shape of the spectrum in that wavelength region. The fact that this electronic transition lies at a lower energy in Re-2 than in Re-1 underlies the better agreement observed between the experimental spectrum of $[Re(CO)_3(bpy)(nHo)]^+$ and theoretical spectrum of Re-2 when compared with that of Re-1.

Conclusions

Two new norharmane Re(I) complexes, Re(I)–nHo, have been obtained successfully. As far as we know this is a beginning of a new family of Re(I) coordination compounds including a β-carbolines as a ligands. Coordination of nHo to Re(I) through pyridine N-atom in solution was evidenced by different spectroscopic techniques. Structural characterization by X-ray diffraction in the solid state confirmed the monodentate coordination of nHo and also showed the three carbonyls are in facial conformation. The octahedral coordination around the central metal is completed by a bidentate L ligand (L = bpy or phen). Structural analysis was deepened by the comparative use of a two mass spectrometry techniques, HRESI and MALDI–MS. Ground state geometry optimization confirmed the more stable structure of *fac*-$[Re(CO)_3(bpy)(nHo)]$-CF_3SO_3 complex. Both DFT and TD-DFT calculations suggest that is highly probable that in fluid solution the nHo coordinated molecule may rotate freely. The set of the most important electronic transitions present in the $[Re(CO)_3(bpy)(nHo)]^+$ complex is comprised of $\pi \rightarrow \pi^*$ electronic transitions centered on bpy and nHo moieties, $LLCT_{nHo\rightarrow COs}$, $MLLCT_{Re(CO)_3\rightarrow bpy}$ and $LLCT_{nHo\rightarrow bpy}$. Moreover, TD-DFT calculations predict the existence of another two intense $MLLCT_{Re(CO)_3\rightarrow nHo}$ electronic transitions.

Both complexes showed high solubility and relative stability in methanol, DMSO and others slightly polar solvents like acetonitrile. Although the solubility in water of these complexes is extremely low, they are soluble in water/ethanol mixtures (*i.e.*, 95% water/5% ethanol). This property is relevant for potential applications in different fields (*e.g.*, biological applications). An interesting feature of both complexes is that the norharmane moiety is coordinated to the metal ion through the pyridinic nitrogen. This would avoid the formation of quaternary βCs (by methyl-transferases), responsible for the neurotoxicity shown by these alkaloids. In this regards, the use of these rhenium complexes instead of free βCs would represent an excellent alternative that should be further explored in a wide range of biomedical applications.

Acknowledgements

This work was supported by CONICET (PIP 1529, PIP 0072CO and PIP 0389), ANPCyT (PME06 2804, PICT06 2315, PICT 2012-0888 and PICT 2012-0423), Universidad de Buenos Aires (X 0055BA) and Universidad Nacional de La Plata (UNLP X611) of Argentina. IM and GTR thank Dr Croce (INIFTA, UNLP, Argentina) for their assistance in FTIR measurements. OEP and GTR thank EE Castellano (USP, Brazil) for help during collection of X-ray diffraction data. The Ultraflex II (Bruker) TOF/TOF mass spectrometer was supported by a grant from ANPCyT (PME 125). IM thanks ANPCyT for research scholarships. FMC, GP, REB, OEP, GAE, EW and GTR are Research Members of CONICET (Argentina).

References

1 J. R. F. Allen and B. R. Holmstedt, *Phytochemistry*, 1980, **19**, 1573–1582.
2 D. Fekkes, A. tuiten, I. Bom and L. Pepplinkhuizen, *Neurosci. Lett.*, 2001, **303**, 145–148.
3 K. Pari, C. Sundari, S. Chandani and D. Balasubramanian, *J. Biol. Chem.*, 2000, **275**, 2455–2462.
4 R. Cao, W. Fan, L. Guo, Q. Mac, G. Zhang, J. Li, X. Chen, Z. Ren and L. Qiu, *Eur. J. Med. Chem.*, 2013, **60**, 135–143.
5 M. L. Alomar, F. A. O. Rasee-Suriani, A. Ganuza, V. M. Cóceres, F. M. Cabrerizo and S. O. Angel, *BCM Res. Notes*, 2013, **6**, 1–6.
6 M. Collins, E. Neafsey, K. Matsubara and R. Cobuzzi Jr., *Brain Res.*, 1992, **570**, 154–160.
7 M. A. Collins and E. J. Neafsey, in *Neurotoxic Factors in Parkinson's Disease and Related Disorders*, ed. A. Storch and M. A. Collins, Kluwer Academic/Plenum Publishers, New York, 2000, 115–129.
8 S. Pavlovic, G. Schulze, C. Wernicke, R. Bonnet, G. Gille, L. Badiali, A. Kaminska, E. Lorenc-Koci, K. Ossowska and H. Rommelspacher, *Neuroscience*, 2006, **139**, 1525–1537.
9 J. Hamann, H. Rommelspacher, A. Storch, H. Reichmann and G. Gille, *J. Neurochem.*, 2006, **98**, 1185–1199.
10 T. A. K. Al-Allaf and L. J. Rashan, *Eur. J. Med. Chem.*, 1998, **33**, 817–820.
11 C. Tan, S. Wu, S. Lai, M. Wang, Y. Chen, L. Zhou, Y. Zhu, W. Lian, W. Peng, L. Ji and A. Xu, *Dalton Trans.*, 2011, **40**, 8611–8621.
12 C. Tan, S. Lai, S. Wu, S. Hu, L. Zhou, Y. Chen, M. Wang, Y. Zhu, W. Lian, W. Peng, L. Ji and A. Xu, *J. Med. Chem.*, 2010, **53**, 7613–7624.
13 M. A. Fox and M. Chanon, *Photoinduced Electron Transfer*, Elsevier, Amsterdam, 1988.
14 M. Grätzel, *Energy Resources Through Photochemistry and Catalysis*, Academic Press, New York, 1983.
15 K. Kalyanasundaram and M. Grätzel, *Photosensitization and Photocatalysis Using Inorganic and Organometallic Compounds*, Kluwer Academic Publishers, Dordrecht, 1993.
16 L. Sacksteder, M. Lee, J. N. Demas and B. A. DeGraff, *J. Am. Chem. Soc.*, 1993, **115**, 8230–8238.
17 A. Vlček, in *Photophysics of Organometallics*, ed. A. J. Lees, Springer, Berlin/Heidelberg, 2010, vol. 29, pp. 73–114.
18 A. Kumar, S.-S. Sun and A. Lees, in *Photophysics of Organometallics*, ed. A. J. Lees, Springer, Berlin/Heidelberg, 2010, vol. 29, pp. 37–71.

19 M. W. Louie, T. Tsz-Fong and K. K. W. Lo, *Inorg. Chem.*, 2011, **50**, 9465–9471.
20 K. Lo, in *Photophysics of Organometallics*, ed. A. J. Lees, Springer, Berlin/Heidelberg, 2010, vol. 29, pp. 73–114.
21 K. K. W. Lo, A. W. T. Choi and W. H. T. Law, *Dalton Trans.*, 2012, **41**, 6021–6047.
22 V. Fernández-Moreira, F. L. Thorp-Greenwood, A. J. Amoroso, J. Cable, J. B. Court, V. Gray, A. J. Hayes, R. L. Jenkins, B. M. Kariuki, D. Lloyd, C. O. Millet, C. F. Williams and M. P. Coogan, *Org. Biomol. Chem.*, 2010, **8**, 3888–3901.
23 G. T. Ruiz, M. P. Juliarena, R. O. Lezna, E. Wolcan, M. R. Feliz and G. Ferraudi, *Dalton Trans.*, 2007, 2020–2029.
24 K. Y. Zhang, K. K. Tso, M. Louie, H. Liu and K. K. Lo, *Organometallics*, 2013, **32**, 5098–5102.
25 J. A. Smith, M. W. George and J. M. Kelly, *Coord. Chem. Rev.*, 2011, **255**, 2666–2675.
26 J. Bhuvaneswari, A. K. Fathima and S. Rajagopal, *J. Photochem. Photobiol., A*, 2012, **227**, 38–44.
27 H. H. Martinez Saavedra, F. Ragone, P. M. David Gara, G. T. Ruiz and E. Wolcan, *J. Phys. Chem. A*, 2013, **117**, 4428–4435.
28 L. He, S. Y. Liao, C. P. Tan, R. R. Ye, Y. W. Xu, M. Zhao, L. N. Ji and Z. W. Mao, *Chem. – Eur. J.*, 2013, **19**, 12152–12160.
29 M. F. Wyatt, *J. Mass Spectrom.*, 2011, **46**, 712–719.
30 G. Petroselli, M. K. Mandal, L. C. Chen, G. T. Ruiz, E. Wolcan, K. Hiraoka, H. Nonami and R. Erra-Balsells, *J. Mass Spectrom.*, 2012, **47**, 313–321.
31 H. Nonami, S. Fukui and R. Erra-Balsells, *J. Mass Spectrom.*, 1997, **32**, 287–296.
32 CrysAlisPro, *Oxford Diffraction Ltfd. version 1.171.33.48 (release 15-09-2009 CrysAlis171.NET)*.
33 Enraf-Nonius, *COLLECT. Nonius BV*, Delft, The Netherlands, 1997–2000.
34 Z. Otwinowski and W. Minor, in *Methods in Enzymology*, ed. C. W. Carter Jr. and R. M. Sweet, Academic Press, New York, 1997, vol. 276, pp. 307–326.
35 A. L. Spek, *PLATON, A Multipurpose Crystallographic Tool*, Utrecht University, Utrecht, The Netherlands, 1998.
36 G. M. Sheldrick, *Acta Crystallogr.*, 2008, **A64**, 112–122.
37 P. Van der Sluis and A. L. Spek, *Acta Crystallogr., Sect. A: Fundam. Crystallogr.*, 1999, **46**, 194–201.
38 F. Ragone, H. H. Martinez Saavedra, G. T. Ruiz, P. M. David Gara and E. Wolcan, *J. Phys. Chem. A*, 2014, **118**, 9661–9674.
39 P. Hohenberg and W. Kohn, *Phys. Rev.*, 1964, **136**, B864–B871.
40 W. Kohn and L. J. Sham, *Phys. Rev.*, 1965, **140**, A1133–A1138.
41 R. G. Parr and W. Yang, *Density Functional Theory of Atoms and Molecules*, Oxford University Press, 1989.
42 M. J. Frisch, *et al.*, *Gaussian 09, Revision A1*, Gaussian, Inc., Wallingford, CT, 2009.
43 A. D. Becke, *J. Chem. Phys.*, 1993, **98**, 5648–5652.
44 P. J. Hay and W. R. Wadt, *J. Chem. Phys.*, 1985, **82**, 270–283.
45 P. J. Hay and W. R. Wadt, *J. Chem. Phys.*, 1985, **82**, 299–310.
46 W. R. Wadt and P. J. Hay, *J. Chem. Phys.*, 1985, **82**, 284–298.
47 R. Bauernschmitt and R. Ahlrichs, *Chem. Phys. Lett.*, 1996, **256**, 454–464.
48 M. E. Casida, C. Jamorski, K. C. Casida and D. R. Salahub, *J. Chem. Phys.*, 1998, **108**, 4439–4449.
49 R. E. Stratmann, G. E. Scuseria and M. J. Frisch, *J. Chem. Phys.*, 1998, **109**, 8218–8224.
50 V. Barone and M. Cossi, *J. Phys. Chem. A*, 1998, **102**, 1995–2001.
51 M. Cossi and V. Barone, *J. Chem. Phys.*, 2001, **115**, 4708–4717.
52 B. Mennucci and J. Tomasi, *J. Chem. Phys.*, 1997, **106**, 5151–5158.
53 U. N. Fagioli, F. S. Garcia Einschlag, C. J. Cobos, G. T. Ruiz, M. R. Féliz and E. Wolcan, *J. Phys. Chem. A*, 2011, **115**, 10979–10987.
54 E. Wolcan, G. Ruiz and M. R. Féliz, *J. Photochem. Photobiol., A*, 1996, **101**, 119–125.
55 J. V. Casper and T. J. Meyer, *J. Phys. Chem.*, 1983, **87**, 952–957.
56 T. A. Oriskovich, P. S. White and H. H. Thorp, *Inorg. Chem.*, 1995, **34**, 1629–1631.
57 R. A. Khan, K. Al-Farhan, A. de Almeida, A. Alsalme, A. Casini, M. Ghazzali and J. Reeddijk, *J. Inorg. Biochem.*, 2014, **140**, 1–5.
58 M. F. Wyatt, B. K. Stein and A. G. Brenton, *Anal. Chem.*, 2006, **78**, 199–206.
59 L. J. Farrugia, *J. Appl. Crystallogr.*, 1997, **30**, 565–566.
60 O. I. Tarzi, M. A. Ponce, F. M. Cabrerizo, S. M. Bonesi and R. Erra-Balsells, *ARKIVOC*, 2005, 295–310.